



Effect of α phase morphology on fatigue crack growth behavior of Ti–5Al–5Mo–5V–1Cr–1Fe alloy

Kui-wai CHEN¹, Su-ping PAN^{1,2}, Hui-qun LIU^{1,3}, Yong JIANG^{1,3}

1. School of Materials Science and Engineering, Central South University, Changsha 410083, China;
2. Advanced Research Center, Central South University, Changsha 410083, China;
3. State Key Laboratory of Powder Metallurgy, Central South University, Changsha 410083, China

Received 15 January 2020; accepted 28 June 2020

Abstract: Taking a Ti–5Al–5Mo–5V–1Cr–1Fe alloy as exemplary case, the fatigue crack growth sensitivity and fracture features with various tailored α phase morphologies were thoroughly investigated using fatigue crack growth rate (FCGR) test, optical microscopy (OM) and scanning electron microscopy (SEM). The tailored microstructures by heat treatments include the fine and coarse secondary α phase, as well as the widmanstatten and basket weave features. The sample with coarse secondary α phase exhibits better comprehensive properties of good crack propagation resistance (with long Paris regime ranging from 15 to 60 MPa·m^{1/2}), high yield strength (1113 MPa) and ultimate strength (1150 MPa), and good elongation (11.6%). The good crack propagation resistance can be attributed to crack deflection, long secondary crack, and tortuous crack path induced by coarse secondary α phase.

Key words: Ti–5Al–5Mo–5V–1Cr–1Fe alloy; α phase; fatigue crack growth; fracture feature

1 Introduction

Near- β Ti–5Al–5Mo–5V–1Cr–1Fe (Ti-55511) alloys are known for the combined advantages of high specific strength, high damage tolerance, and strong corrosion resistance, and are suitable for use as aircraft landing gear, wing and engineer blades [1,2]. For such applications, one of the key properties to be concerned is fatigue resistance. The effects of different microstructures on fatigue crack growth behavior of Ti-based alloys, such as the widmanstatten, the basket-weave, and the equiaxed microstructure, have attracted major attention under the damage tolerance design concept [3–6]. SHI et al [3] studied the fatigue crack growth rate of a Ti–5Al–5Mo–5V–1Cr–1Fe alloy with different basket-weave microstructures, and found that the

long and thick α lamellar features were the most effective in deflecting the main crack. SHEN et al [4] studied the fatigue crack growth of a Ti–6Al–2Sn–4Zr–2Mo–0.1Si alloy with an equiaxed microstructure, a duplex microstructure containing elongated primary α grains, or a widmanstatten microstructure, and found that widmanstatten microstructure led to a tortuous crack path and hence the highest resistance to fatigue crack growth. SHI et al [5] further suggested the colony size and the α platelet thickness of a widmanstatten microstructure as two critical factors in influencing the FCG behavior of Ti–6Al–2Zr–2Sn–3Mo–1Cr–2Nb alloys, for the main crack was often observed to propagate along the α platelets and/or the colony boundaries.

In near- β titanium alloy, secondary α phase precipitates after solid solution and aging treatments.

Foundation item: Project (U1867201) supported by the National Natural Science Foundation of China; Project supported by State Key Laboratory of Powder Metallurgy, Central South University, China

Corresponding author: Hui-qun LIU, E-mail: liuhuiqun@csu.edu.cn; Yong JIANG, E-mail: yjiang@csu.edu.cn
DOI: 10.1016/S1003-6326(20)65392-4

In recent years, the important influence of secondary α phase on the strength, elongation, and fracture toughness of Ti alloys has become a new research focus [7–10]. For instance, the $\alpha+\beta$ solution treated and aged Ti–6Cr–5Mo–5V–4Al alloy obtained a high strength of 1500 MPa with fine-size secondary α phase, while the β solution treated and aged counterpart alloy had a low strength with coarse secondary α phase [7]. Coarse secondary α phase, however, can benefit in improving both ductility and fracture toughness of a Ti–5Al–5Mo–5V–3Cr–1Zr alloy by deflecting the crack paths [8]. Also, the re-dissolving of secondary α phase during uniaxial fatigue led to a reduction in both the strength and elongation of a Ti-55511 alloy [9]. However, the roles of secondary α phase on fatigue crack growth rate among various microstructures, such as duplex and different widmanstatten microstructures of Ti alloys remain still unclear.

In this work, the effects of fine and coarse secondary α phase, along with the typical and inhomogeneous widmanstatten microstructures, on fatigue crack growth behavior of Ti alloys were thoroughly studied. The mechanisms for fatigue fracture and crack propagation paths were also discussed. Based on our improved knowledge, the strategy for achieving good comprehensive properties (high crack growth resistance, strength and elongation) through tailoring secondary α phase was proposed and further validated. All these results can provide a useful guidance for developing high-strength and high-toughness Ti alloys with desired fatigue resistances.

2 Experimental

2.1 Materials

The forged blank of Ti-55511 alloy used in this work was provided by Hunan GoldSky Titanium Industry Technology Company Ltd., China. The as-received microstructure consists of equiaxed α phase, lamellar α phase and transformed β phase, as shown in Fig. 1. The $\beta/\alpha+\beta$ transus temperature of the alloy was identified to be (875 ± 5) °C. To obtain different secondary α -phase features, two specimens were heated at 830 °C (under $\beta/\alpha+\beta$ phase transus temperature) for 4 h followed by air

cooling, and then aged at 600 °C and 650 °C for 16 h respectively. To obtain different lamellar α features, other two samples were heated at 950 and 895 °C for 2 h respectively, followed by furnace cooling and aging at 600 °C for 16 h and air cooling. The resulted four different heat-treated samples were referred as A, B, C and D in Table 1, respectively.

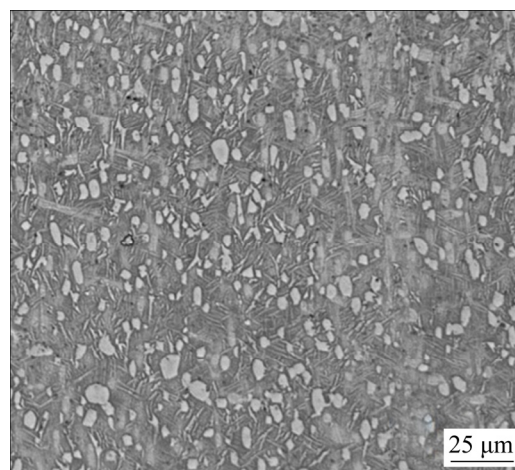


Fig. 1 As-received microstructure of Ti-55511 alloy

Table 1 Samples and heat treatment processes for Ti-55511 alloy

Sample No.	Heat treatment condition
A	(830 °C, 4 h, AC)+(600 °C, 16 h, AC)
B	(830 °C, 4 h, AC)+(650 °C, 16 h, AC)
C	(950 °C, 2 h, FC)+(600 °C, 16 h, AC)
D	(895 °C, 2 h, FC)+(600 °C, 16 h, AC)

2.2 Tensile and fatigue tests

Three tensile specimens with a thickness of 2 mm for each heat treatment condition were used to test room temperature tensile properties. The standard compact tension (CT) specimens with a thickness of 3 mm were used to test fatigue crack growth rates on a MTS Landmark Testing Machine with servo-hydraulic system. Dimensions of test specimens are shown in Fig. 2. The notch was prepared and perpendicular to the loading direction. Pre-crack was introduced with a length of 2 mm and then FCGR tests were performed at a stress ratio of 0.1 and a frequency of 10 HZ.

2.3 Microstructure characterization

The microstructure and fracture morphology

under four different heat treatments were observed by a LEICA DM4M optical microscope and scanning electron microscopy. SEM analysis was performed using TESCAN MIRA3 and ZEISS EVO MA10. Further observations on crack propagation paths and microstructure surrounding cracks were also carried out in details.

3 Results and discussion

3.1 Microstructure

The OM and SEM microstructures of heat-treated Ti-55511 alloy samples are shown in Fig. 3.

For Samples A and B, microstructures consisted of primary α phase and secondary α phase as shown in Figs. 3(a) and (b), respectively. The thickness of secondary α phase in Sample B was obviously larger than that in Sample A. The microstructure of Sample C showed inhomogeneous structure feature in Fig. 3(c). Grain boundary widmanstatten microstructure (α_{WGB}) existed near grain boundaries, while intragranular widmanstatten microstructure (α_{in}) with randomly distributed α platelets grew inside grains. After solid solution, α phase precipitated and formed α_{WGB} feature in the following furnace cooling. However, due to the

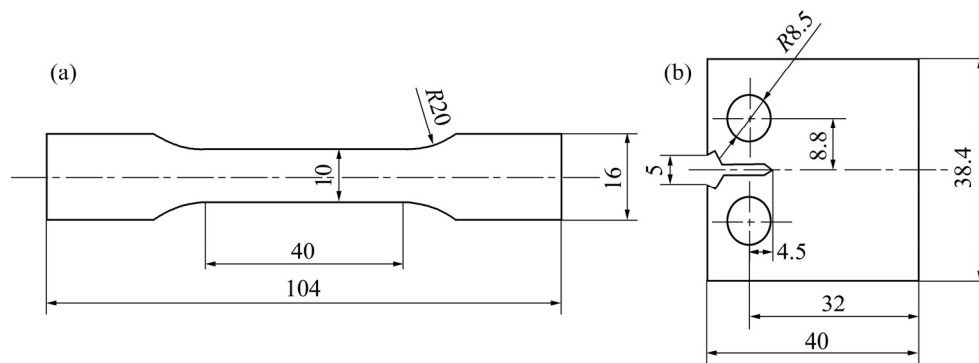


Fig. 2 Schematic diagram of tensile sample (a), fatigue CT sample and their dimensions (b) (unit: mm)

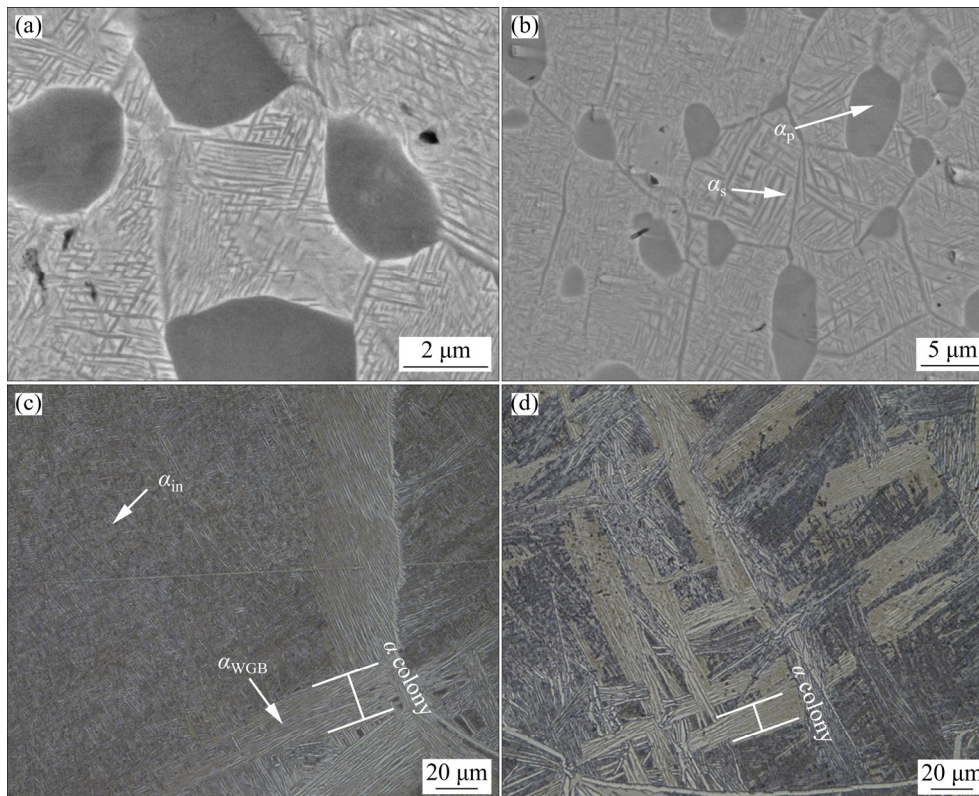


Fig. 3 SEM (a, b) and OM (c, d) images of four heat-treated samples: (a) Sample A; (b) Sample B; (c) Sample C; (d) Sample D

large β grain size in Sample C, α_{WGB} could not penetrate the entire β grain and finally came into contact with other α_{WGB} nearby. Simultaneously, α_{in} was formed within β grain and grew up. The microstructure of Sample D exhibited typical lamellar feature in Fig. 3(d). The average primary β grain size, α platelet thickness, colony size and secondary α phase thickness were quantitatively measured over 100 grains by Nano Measurer 1.2 software in all cases [11], and the microstructure parameters are listed in Table 2.

3.2 Tensile properties

Figures 4 and Table 3 show the tensile properties of four samples. It can be seen that, compared with the other three samples, Sample A has the highest ultimate strength (σ_b) 1308 MPa and yield strength ($\sigma_{0.2}$) 1281 MPa. The existence of equiaxed α phase and fine secondary α phase is responsible for high strength [12]. Sample B shows medium ultimate strength (1150 MPa) and the best elongation (11.6%). Thus, Sample B has an attractive combination of strength and ductility. Compared with Sample D, Sample C has higher ultimate strength and lower elongation. Short effective slip length of α platelets in α_{in} microstructure results in the strength improvement of Sample C [13–15].

3.3 Fatigue crack growth rate (FCGR)

Figure 5 shows the FCGR curves of four heat-treated Ti-55511 alloy samples. Evidently, Sample A has higher FCGR, shorter steady crack propagation stage and faster quick crack propagation stage than Sample B. Increasing the aging temperature can effectively enhance the fatigue crack resistance of duplex microstructure. The FCGR of Sample C is lower than the other three samples. Large colony size in α_{WGB}

microstructure [16,17] and large misorientation in α_{in} microstructure [18,19] may be two important factors in enhancing fatigue crack growth resistance of Sample C. The Paris regime of the FCGR curve is generally characterized as

$$d\alpha/dN=C'(\Delta K)^m \quad (1)$$

where α is the crack length, N is the number of loading cycles, ΔK is the stress intensity factor range, C' and m are the Paris coefficient and Paris exponent, respectively. The values of C' and m are summarized in Table 4. The Paris exponents m for Samples A, B, C and D are 3.33, 2.41, 2.13 and 2.49, respectively. Different values of m also indicate the microstructure effects on fatigue crack growth resistance of Ti-55511 alloy.

3.4 SEM fractograph analysis

Figure 6 shows the SEM fractographs of Sample A. Figure 6(a) exhibits the whole fracture morphology. In the near threshold regime, crystallographic-faceted mode is dominant and abundant facets can be found in Fig. 6(b). In the Paris regime, fatigue striations appear due to the alternating slip process with increasing ΔK [4]. However, only some regions own fatigue striations. The cleavage facet fracture mode is still dominant in the Paris regime as shown in Figs. 6(c) and (d). It is worthy noting that the Paris regime (Figs. 6(c) and (d)) is much shorter than the high ΔK regime (Fig. 6(e)), which is consistent with the FCGR result above. In the high ΔK regime, a combination of facets and ductile dimples was observed (Fig. 6(e)).

Figure 7 shows the SEM fractograph of Sample B. It can be found that the fracture surface of Sample B (Fig. 7(a)) is rougher than that of Sample A (Fig. 6(a)). Higher undulation depth implies larger deflection of cracks and additional

Table 2 Statistical microstructural parameters of Samples A, B, C and D

Sample No.	Microstructure	β grain size/ μm	α colony size/ μm	α plate size/ μm	Secondary α size/ μm
A	Duplex	7 \pm 3	–	–	0.08 \pm 0.02
B	Duplex	8 \pm 2	–	–	0.18 \pm 0.06
C	α_{WGB}	440 \pm 203	22 \pm 21	0.75 \pm 0.22	–
	α_{in}		3 \pm 1	0.41 \pm 0.08	
D	Widmanstätten	289 \pm 139	11 \pm 5	0.78 \pm 0.27	–

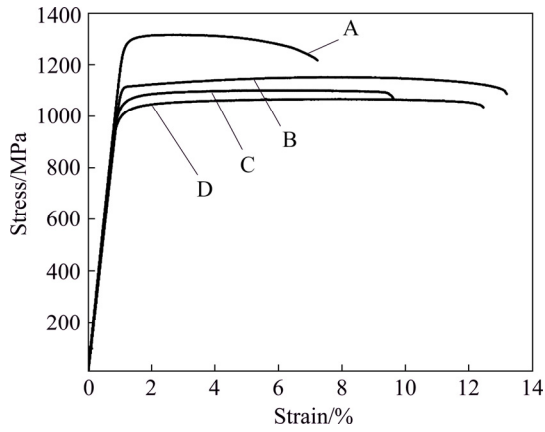


Fig. 4 Stress–strain curves of Samples A, B, C and D

Table 3 Tensile properties of four heat-treated samples

Sample No.	$\sigma_{0.2}$ /MPa	σ_b /MPa	δ /%
A	1281±11	1308±12	4.9±0.5
B	1113±2	1150±3	11.6±1.8
C	1039±3	1098±6	7.8±1.0
D	994±14	1066±8	10.9±0.2

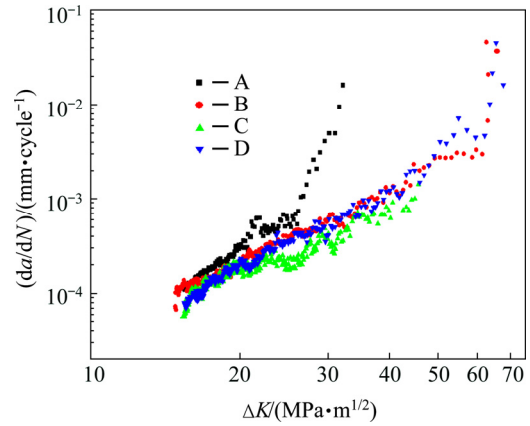


Fig. 5 Fatigue crack growth rates of four heat-treated samples

Table 4 Fatigue crack growth parameters of four heat-treated samples

Sample No.	C'	m
A	1.50×10^{-8}	3.33
B	1.60×10^{-7}	2.41
C	2.67×10^{-7}	2.13
D	1.14×10^{-7}	2.49

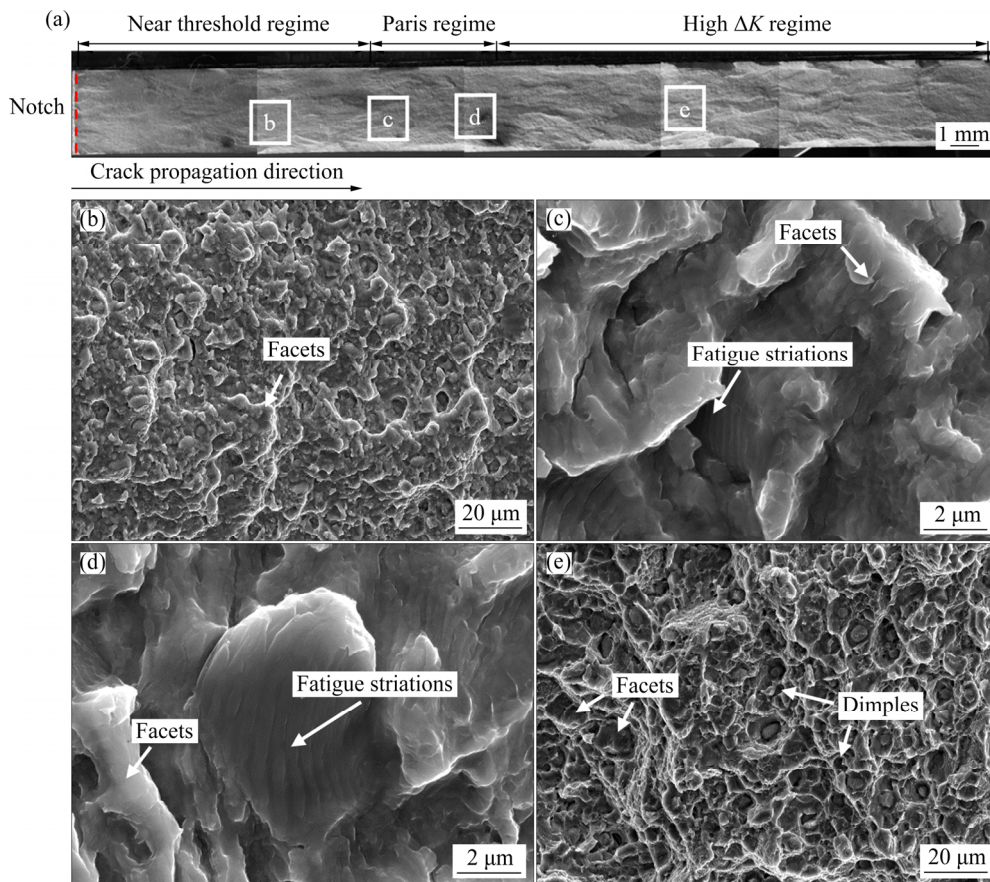


Fig. 6 SEM fatigue fractographs of Sample A: (a) Whole morphology; (b) Near threshold regime; (c, d) Paris regime; (e) High ΔK regime

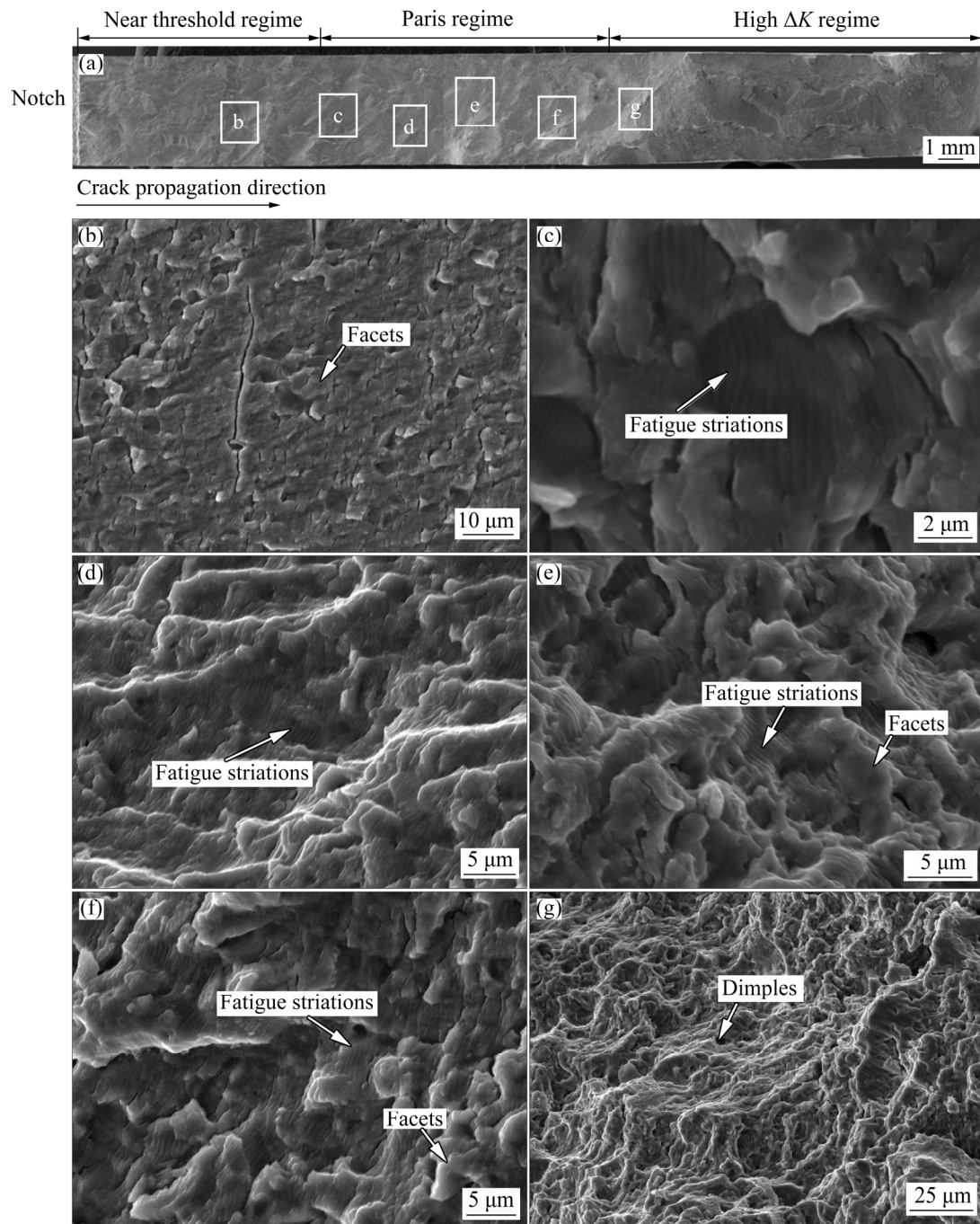


Fig. 7 SEM fatigue fractographs of Sample B: (a) Whole morphology; (b) Near threshold regime; (c, d) Low Paris regime; (e, f) Upper Paris regime; (g) High ΔK regime

energy consuming. Crystallographic-faceted mode was also observed in the near threshold regime (Fig. 7(b)). However, in the Paris regime, there is a difference between Samples A and B. As the ΔK increases, lots of fatigue striations appear, indicating that the fatigue striation fracture mode becomes dominant. The striation spacing increases from 0.36 μm (Fig. 7(c)) to 0.50 μm (Fig. 7(f)). PILCHAK [20] found that the FCGR of facet

fracture mode could be two orders of magnitude higher than striation fracture mode in a single-phase Ti-7Al alloy. Thus, the transition of primary fracture mode contributed to the significant enhancement of fatigue crack growth resistance of Sample B.

Figures 8 and 9 show the SEM fractographs of Samples C and D, respectively. In the near threshold regime, Sample C (Fig. 8(b)) and Sample

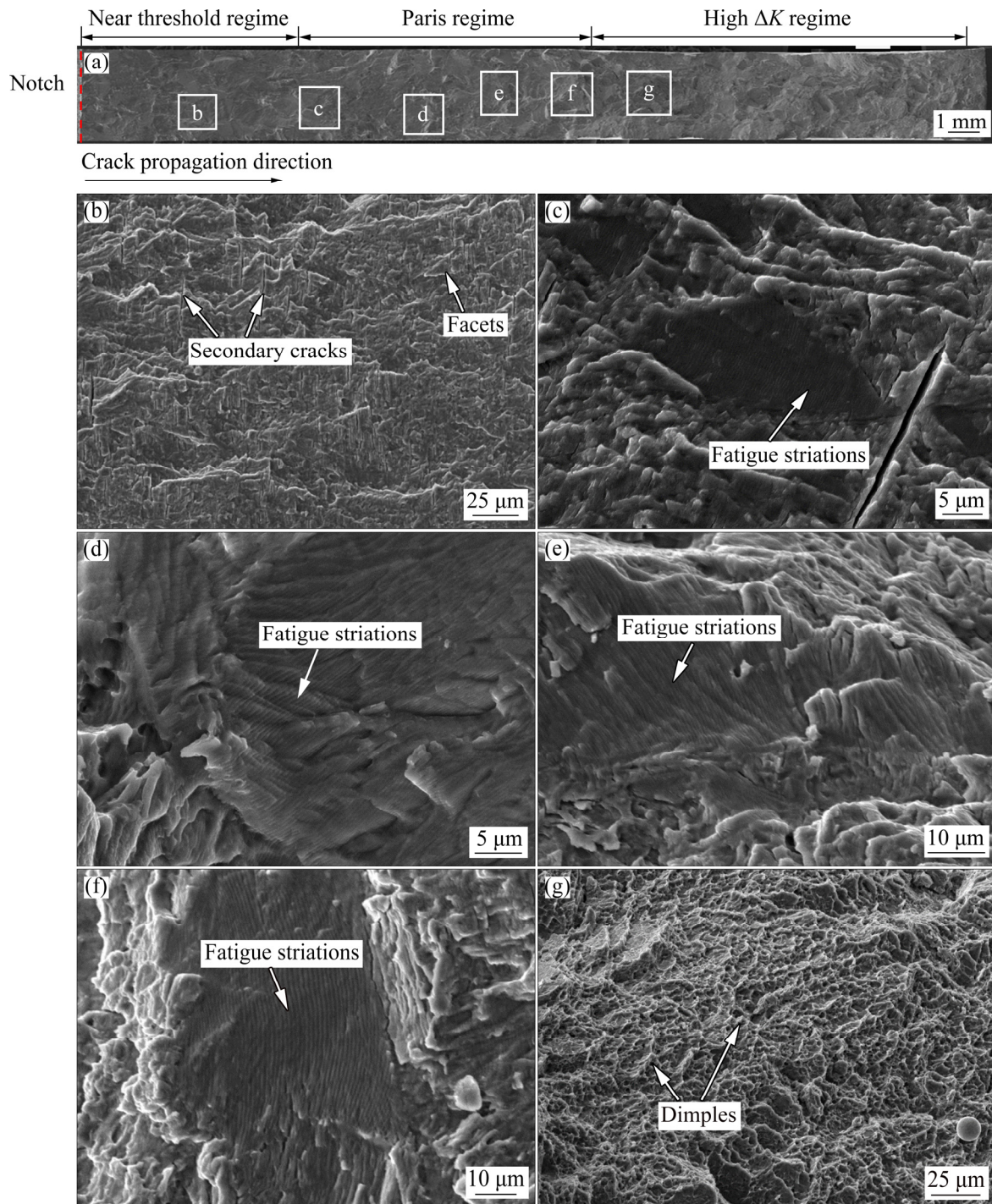


Fig. 8 SEM fatigue fractographs of Sample C: (a) Whole morphology; (b) Near threshold regime; (c, d) Low Paris regime; (e, f) Upper Paris regime; (g) High ΔK regime

D (Fig. 9(b)) are dominated by cleavage facet fracture. Meanwhile, secondary cracks of Sample C (Fig. 8(b)) are much more than those of Sample D (Fig. 9(b)). Fatigue striations with increasing spacing can be observed in the Paris regime for two samples. The striation spacing of Sample C increases from 0.27 μm (Fig. 8(c)) to 0.99 μm

(Fig. 8(f)), while the striation spacing of Sample D increases from 0.31 μm (Fig. 9(c)) to 1.27 μm (Fig. 9(f)). Relative wider fatigue striation spacing of Sample D may be due to the effects of local microstructure and crystal orientation. Figures 8(g) and 9(g) are characterized by dimples, similar to tensile final fracture features.

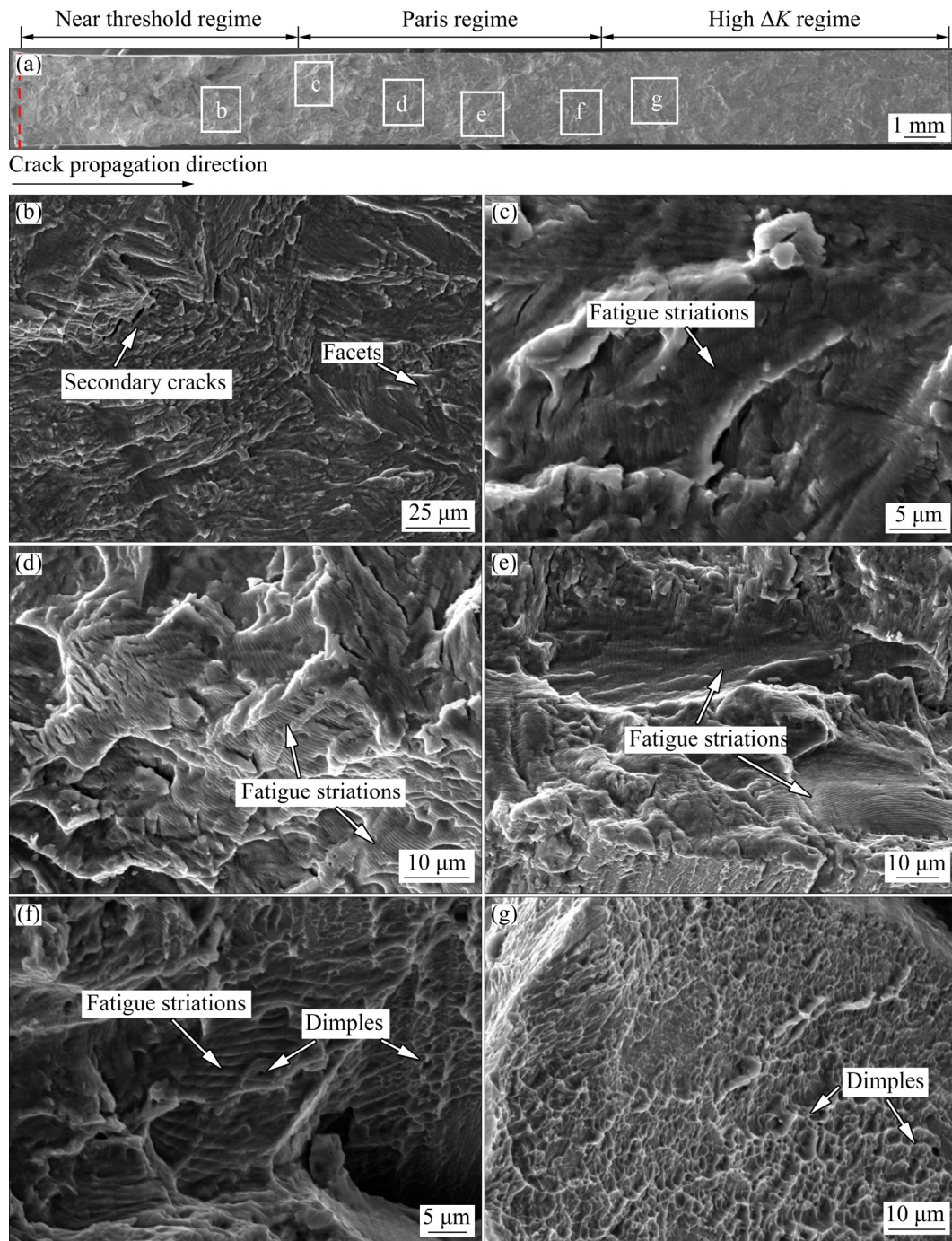


Fig. 9 SEM fatigue fractographs of Sample D: (a) Whole morphology; (b) Near threshold regime; (c, d) Low Paris regime; (e, f) Upper Paris regime; (g) High ΔK regime

3.5 Crack propagation path

Figures 10 and 11 show the crack propagation paths of Samples A and B, respectively. It can be seen that the fatigue crack propagation path of Sample B (Fig. 11(a)) is more tortuous than that of Sample A (Fig. 10(a)). Rough fatigue crack path and high undulation require more energy. Thus, it provides a positive contribution to crack growth

resistance of Sample B. For Sample A, when the main fatigue crack encounters a primary α grain, there are two types of fatigue crack growth behaviors. The fatigue crack can cut through the primary α grain (Fig. 10(b)) or bypass the primary α grain (Fig. 10(c)). Similar results of the Ti-6Al-2Sn-4Zr-2Mo alloy have been reported by ZHOU et al [21]. In some cases, crack deflection (Fig. 10(d))

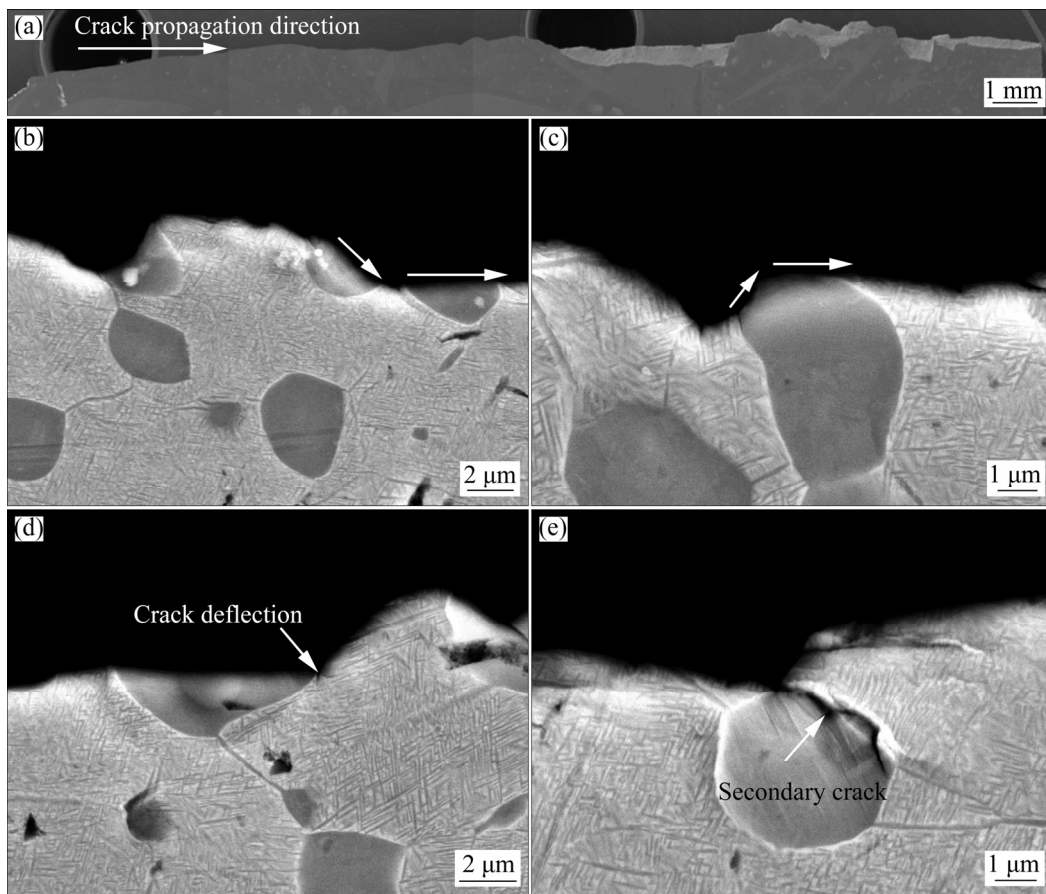


Fig. 10 Crack profiles of Sample A: (a) Whole crack propagation path; (b) Cutting through primary α phase; (c) Bypass primary α phase; (d) Crack deflection at primary α grain boundary; (e) Secondary crack along primary α grain boundary

and secondary crack propagating along primary α grain boundary (Fig. 10(e)) can be observed. It is well known that the local driving force at crack tip can be effectively reduced by the crack deflection and secondary crack [22]. However, the area percentage of primary α phase is only about 17% and provides limited fatigue crack resistance. For Sample B, the secondary α phase is more than twice thicker than that of Sample A. When the main fatigue crack encounters a coarse secondary α phase, it deflects and propagates in a more tortuous path, as shown in Figs. 11(b) and (c). In addition, large secondary crack can be found in Fig. 11(f). Thus, from the discussions above, the fatigue crack growth rate of Sample B is effectively reduced by crack deflection and secondary crack.

For Sample C, secondary crack can propagate to a long distance in α_{in} microstructure, as shown in Fig. 12(d). For Sample D, secondary crack is impeded by the colony boundaries and can only

extend to a short distance, as shown in Fig. 13(c). Similar report can be seen in Ref. [23]. The average α colony size of Sample C is about twice larger than that of Sample B, which can weaken the hindering effect of colony boundaries on fatigue crack propagation [23,24]. In some cases, the fatigue crack cannot cut straightly through a colony where the aligned α platelets behave like a single crystal [25,26]. As a result, the fatigue crack deflects (Fig. 13(b)) or propagates in a zig-zag path (Fig. 12(d)), which consumes crack tip stress and strain field energy [27,28]. Besides, a tortuous fatigue crack propagation path (Fig. 12(c)) accompanied with substantial secondary cracks (Fig. 12(e)) in α_{in} microstructure can be observed, which may be due to the large misorientation of colony boundaries [19,29,30]. Therefore, α_{WGB} microstructure and α_{in} microstructure can serve as two important contributions to improve fatigue crack growth resistance of Sample C.

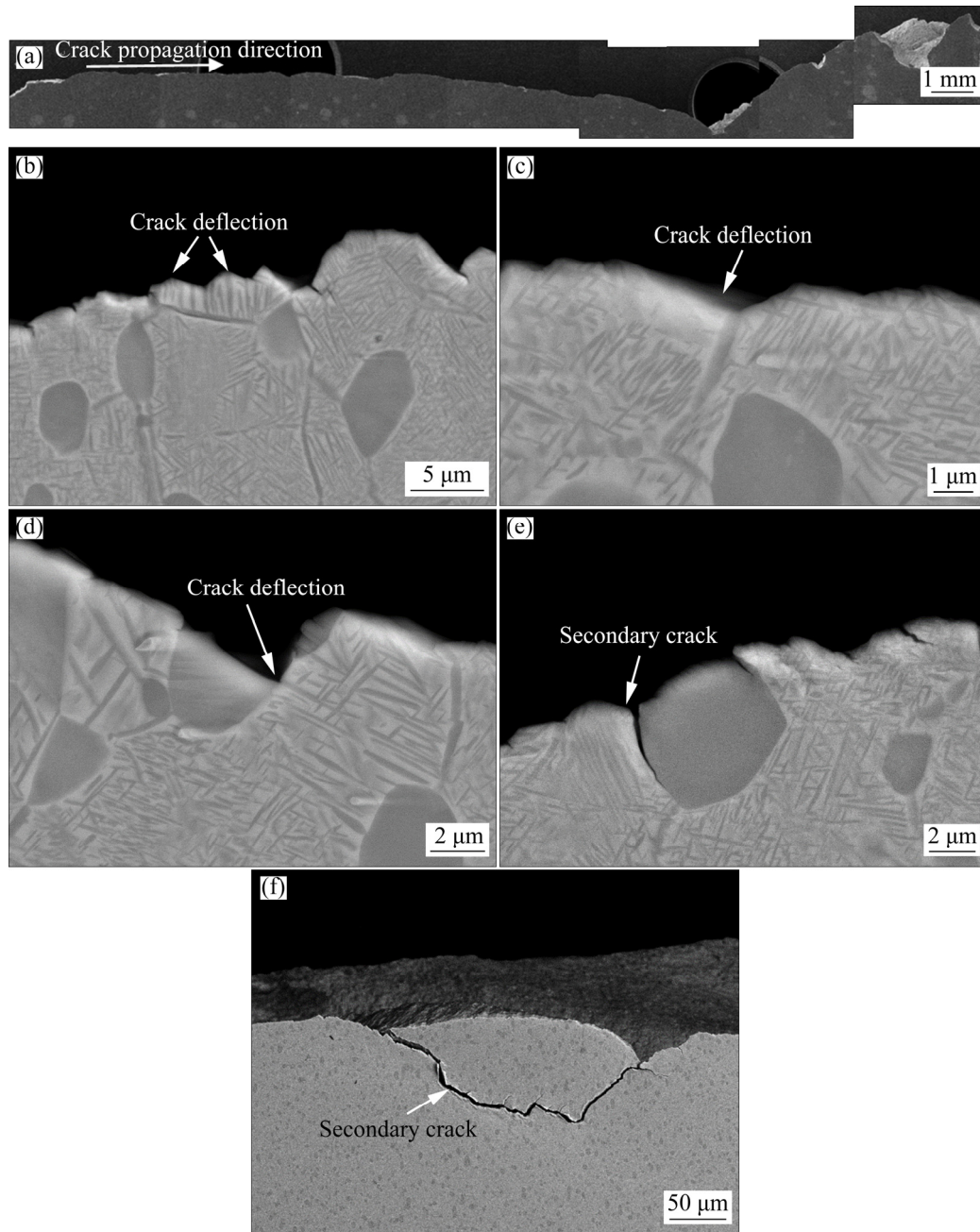


Fig. 11 Crack profiles of Sample B: (a) Whole crack propagation path; (b, c) Crack deflection induced by secondary α phase; (d) Crack deflection at primary α grain boundary; (e) Secondary crack along primary α grain boundary; (f) Long secondary crack

4 Conclusions

(1) The thickness of secondary α phase increases with increasing aging temperature and the widmanstatten microstructure becomes inhomogeneous at a higher solution temperature.

(2) The sample with coarse secondary α phase exhibits better comprehensive properties of high

strength, good elongation and good crack propagation resistance.

(3) Coarse secondary α phase can result in the crack deflection, long secondary crack and tortuous crack path. Inhomogeneous widmanstatten microstructure shows the best crack propagation resistance, for α_{WGB} microstructure and α_{in} microstructure can serve as two important contributions to improve fatigue crack growth resistance.

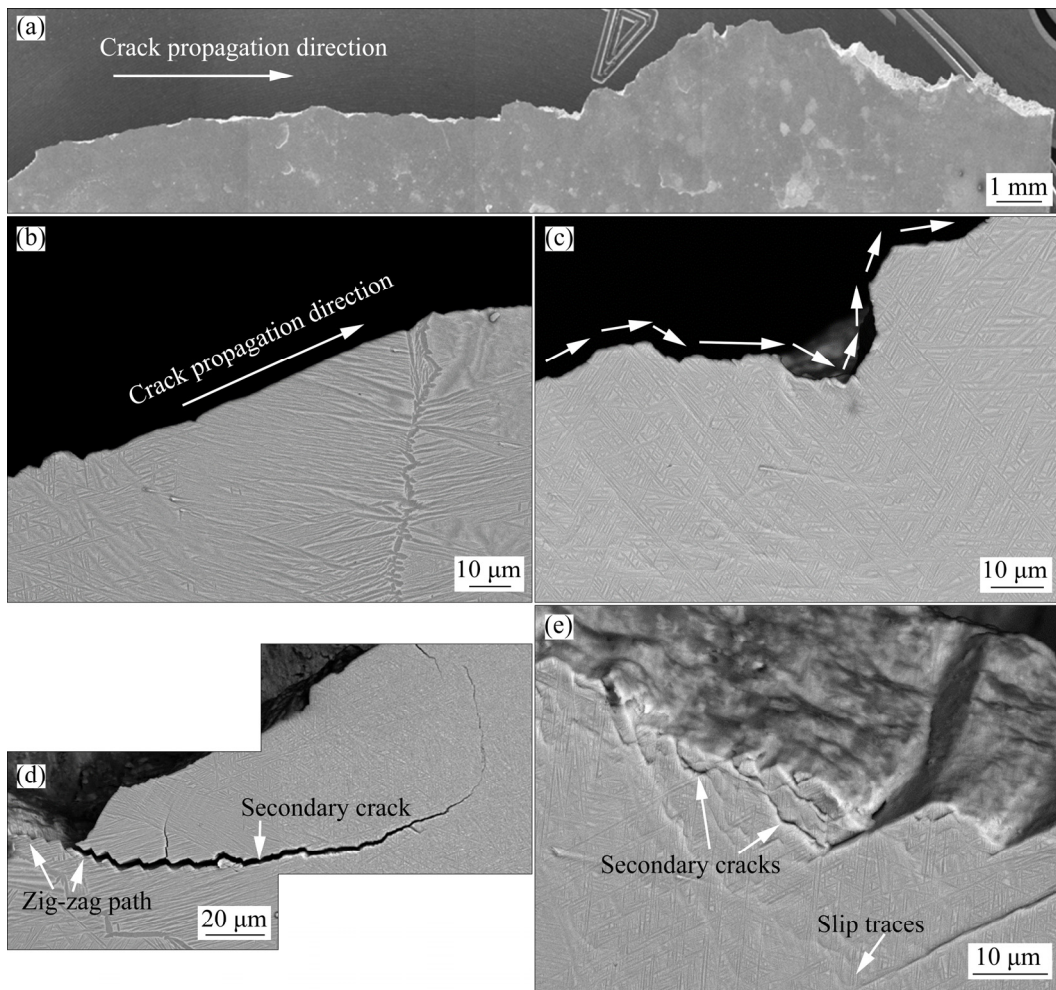


Fig. 12 Crack profiles of Sample C: (a) Whole crack propagation path; (b, c) Fatigue crack propagation path in α_{WGB} and α_{in} microstructure, respectively; (d) Long secondary crack with zig-zag path; (e) Secondary cracks and slip traces in α_{in} microstructure

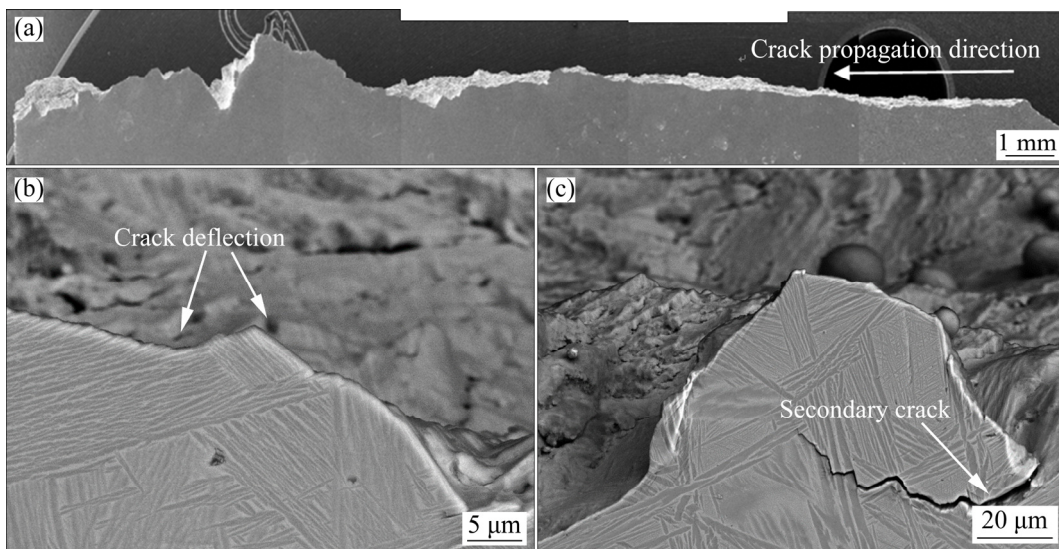


Fig. 13 Crack profiles of Sample D: (a) Whole crack propagation path; (b) Crack deflection in colonies; (c) Secondary crack in colonies

Acknowledgments

The authors thank Hunan GoldSky Titanium Industry Technology Company Ltd., for providing the raw materials used in this study.

References

- [1] ARRIETA A J, STRIZ A G. Optimal design of aircraft structures with damage tolerance requirements [J]. *Structural and Multidisciplinary Optimization*, 2005, 30: 155–163.
- [2] TOOR P M. A review of some damage tolerance design approaches for aircraft structures [J]. *Engineering Fracture Mechanics*, 1973, 5: 837–880.
- [3] SHI X H, ZENG W D, SHI C L, WANG H J, JIA Z Q. Study on the fatigue crack growth rates of Ti–5Al–5Mo–5V–1Cr–1Fe titanium alloy with basket-weave microstructure [J]. *Materials Science and Engineering A*, 2015, 621: 143–148.
- [4] SHEN W, SOBOYEJO W O, SOBOYEJO A B D. An investigation on fatigue and dwell-fatigue crack growth in Ti–6Al–2Sn–4Zr–2Mo–0.1Si [J]. *Mechanics of Materials*, 2004, 36: 117–140.
- [5] SHI X H, ZENG W D, SHI C L, WANG H J, JIA Z Q. The effects of colony microstructure on the fatigue crack growth behavior for Ti–6Al–2Zr–2Sn–3Mo–1Cr–2Nb titanium alloy [J]. *Materials Science and Engineering A*, 2015, 621: 252–258.
- [6] LI Ming-bing, ZHU Zhi-shou, WANG Xin-nan, ZHU Li-wei, FEI Yue, SHANG Guo-qiang, LI Jing. Influence of microstructure on high cycle fatigue properties of TC32 titanium alloy [J]. *Transactions of Nonferrous Metals Society of China*, 2016, 26: 1886–1892.
- [7] LI C L, MI X J, YE W J, HUI S X, YU Y, WANG W Q. A study on the microstructures and tensile properties of new beta high strength titanium alloy [J]. *Journal of Alloys and Compounds*, 2013, 550: 23–30.
- [8] WU C, ZHAN M. Effect of solution plus aging heat treatment on microstructural evolution and mechanical properties of near- β titanium alloy [J]. *Transactions of Nonferrous Metals Society of China*, 2019, 29: 997–1006.
- [9] PAN S P, LIU H Q, CHEN Y Q, CHEN K W, YI D Q. α_s dissolving induced mechanical properties decay in Ti-55511 alloy during uniaxial fatigue [J]. *International Journal of Fatigue*, 2020, 132: 105372.
- [10] SHI Z F, GUO H Z, ZHANG J W, YIN J N. Microstructure–fracture toughness relationships and toughening mechanism of TC21 titanium alloy with lamellar microstructure [J]. *Transactions of Nonferrous Metals Society of China*, 2018, 28: 2440–2448.
- [11] WU G Q, SHI C L, SHA W, SHA A X, JIANG H R. Microstructure and high cycle fatigue fracture surface of a Ti–5Al–5Mo–5V–1Cr–1Fe titanium alloy [J]. *Materials Science and Engineering A*, 2013, 575: 111–118.
- [12] LI C L, MI X J, YE W J, HUI S X, YU Y, WANG W Q. Effect of solution temperature on microstructures and tensile properties of high strength Ti–6Cr–5Mo–5V–4Al alloy [J]. *Materials Science and Engineering A*, 2013, 578:103–109.
- [13] ZHAO Z, CHEN J, LU X, TAN H, LIN X, HUANG W. Formation mechanism of the α variant and its influence on the tensile properties of laser solid formed Ti–6Al–4V titanium alloy [J]. *Materials Science and Engineering A*, 2017, 691: 16–24.
- [14] ZHU Y, JIA L, TIAN X, WANG H, DONG L. Microstructure and mechanical properties of hybrid fabricated Ti–6.5Al–3.5Mo–1.5Zr–0.3Si titanium alloy by laser additive manufacturing [J]. *Materials Science and Engineering A*, 2014, 607: 427–434.
- [15] TAN C, LI X, SUN Q, XIAO L, ZHAO Y, SUN J. Effect of α -phase morphology on low-cycle fatigue behavior of TC21 alloy [J]. *International Journal of Fatigue*, 2015, 75: 1–9.
- [16] YODER G R, EYLLON D. On the effect of colony size on fatigue crack growth in Widmanstätten structure $\alpha+\beta$ titanium alloys [J]. *Metallurgical Transactions A*, 1979, 10: 1808–1810.
- [17] SINHA V, SOBOYEJO W O. An investigation of the effects of colony microstructure on fatigue crack growth in Ti–6Al–4V [J]. *Materials Science and Engineering A*, 2001, 319: 607–612.
- [18] FAN J K, LI J S, KOU H C, HUA K, TANG B. The interrelationship of fracture toughness and microstructure in a new near β titanium alloy Ti–7Mo–3Nb–3Cr–3Al [J]. *Materials Characterization*, 2014, 96: 93–99.
- [19] BIROSCA S, BUFFIERE J Y, KARADGE M, PREUSS M. 3-D observations of short fatigue crack interaction with lamellar and duplex microstructures in a two-phase titanium alloy [J]. *Acta Materialia*, 2011, 59: 1510–1522.
- [20] PILCHAK A L. Fatigue crack growth rates in alpha titanium: Faceted vs. striation growth [J]. *Scripta Materialia*, 2013, 68: 277–280.
- [21] ZHOU H W, LIU H Q, YI D Q, XIAO Y, ZHAO X L, WANG J, GAO Q. Effect of α phase on fatigue crack growth of Ti-6242 alloy [J]. *Journal of Iron and Steel Research, International*, 2017, 24: 811–822.
- [22] ZHANG Z, HU Z F, FAN L K, WANG B. Low cycle fatigue behavior and cyclic softening of P92 ferritic-martensitic steel [J]. *Journal of Iron and Steel Research, International*, 2015, 22: 534–542.
- [23] LUO Z J, SHEN J C, SU H, DING Y H, YANG C F, ZHU X. Effect of substructure on toughness of lath martensite/bainite mixed structure in low-carbon steels [J]. *Journal of Iron and Steel Research, International*, 2010, 17: 40–48.
- [24] WEN X, WAN M, HUANG C, LEI M. Strength and fracture toughness of TC21 alloy with multi-level lamellar microstructure [J]. *Materials Science and Engineering A*, 2019, 740–741: 121–129.
- [25] QIU J, FENG X, MA Y, LEI J, LIU Y, HUANG A, RUGG D, YANG R. Fatigue crack growth behavior of beta-annealed Ti–6Al–2Sn–4Zr–xMo (x=2, 4 and 6) alloys: Influence of microstructure and stress ratio [J]. *International Journal of Fatigue*, 2016, 83: 150–160.
- [26] JIN O, MALL S. Effects of microstructure on short crack growth behavior of Ti–6Al–2Sn–4Zr–2Mo–0.1Si alloy [J]. *Materials Science and Engineering A*, 2003, 359: 356–367.
- [27] YODER G R, COOLEY L A, CROOKER T W. Fatigue crack propagation resistance of beta-annealed Ti–6Al–4V

- alloys of differing interstitial oxygen contents [J]. Metallurgical Transactions A, 1978, 9: 1413–1420.
- [28] MINGBING L, ZHISHOU Z, XINNAN W, LIWEI Z, GUOQIANG S, JING L, GECHEN L. Fatigue crack growth behaviors in Novel TC32 titanium alloy with bimodal and basket-wave microstructures [J]. Materials Science Forum, 2019, 944: 120–126.
- [29] WANG P, BHATE N, CHAN K S, KUMAR K S. Colony boundary resistance to crack propagation in lamellar Ti–46Al [J]. Acta Materialia, 2003, 51: 1573–1591.
- [30] HUANG C, ZHAO Y, XIN S, ZHOU W, LI Q, ZENG W, TAN C. High cycle fatigue behavior of Ti–5Al–5Mo–5V–3Cr–1Zr titanium alloy with bimodal microstructure [J]. Journal of Alloys and Compounds, 2016, 682: 107–116.

α 相形貌对 Ti–5Al–5Mo–5V–1Cr–1Fe 合金 疲劳裂纹扩展行为的影响

陈葵外¹, 潘素平^{1,2}, 刘会群^{1,3}, 江勇^{1,3}

1. 中南大学 材料科学与工程学院, 长沙 410083;
2. 中南大学 高等研究中心, 长沙 410083;
3. 中南大学 粉末冶金国家重点实验室, 长沙 410083

摘要: 采用疲劳裂纹扩展测试、金相显微镜分析和扫描电子显微镜分析方法研究不同 α 相形貌对 Ti–5Al–5Mo–5V–1Cr–1Fe 合金的疲劳裂纹扩展敏感性及其断裂特征的影响。通过热处理制备的显微组织包括细小和粗大的次生 α 相组织、魏氏组织和网篮组织。具有粗大次生 α 相的组织具有最好的综合性能, 包括良好的裂纹扩展抗性 (Paris 区为 15~60 MPa·m^{1/2})、高的屈服强度(1113 MPa)和抗拉强度(1150 MPa), 以及良好的伸长率(11.6%)。良好的裂纹扩展抗性归因于粗大次生 α 相引起的裂纹偏折、长二次裂纹和曲折的裂纹路径。

关键词: Ti–5Al–5Mo–5V–1Cr–1Fe 合金; α 相; 疲劳裂纹扩展; 断裂特征

(Edited by Xiang-qun LI)